Detection of O(^{1}D) Produced in the Photodissociation of O_2 in the Schumann−Runge Continuum

J. B. Nee*,†,‡ and P. C. Lee†

Department of Physics and Department of Chemistry, National Central University, Chung-Li, Taiwan, Republic of China 320

Received: February 4, 1997; In Final Form: June 23, 1997[⊗]

O(^{1}D) produced from O_2 by photodissociation in the Schumann−Runge continuum was studied. The metastable atom O(^{1}D) was detected by observing the 762 nm fluorescence from O_2(b $^1\Sigma_g^+$) generated by the energy transfer process O(^{1}D) + O_2 → O + O_2(b $^1\Sigma_g^+$). A quantum yield of unity was found in the wavelength range 139−175 nm. O(^{1}D) was detected at wavelengths longer than the threshold at 175 nm with reduced quantum yields due to excitations of molecules in the high rotational states. The quantum yields vary from 1 in the range 130−139 nm, resulting from crossing of the state $^3\Sigma_u^-$ with $^3\Pi_u$. The absorption spectra for both states were determined. The peaks for maxima and minima absorptions were compared with previous experimental and theoretical results.

1. Introduction

The electronic transition B $^3\Sigma_u^-$ ← X $^3\Sigma_g^-$ of O_2 is responsible for the photoabsorption of the Schumann−Runge bands at 175−195 nm and the Schumann−Runge continuum (SRC) at 135−175 nm. The continuous absorption in the SRC is due to excitation to energy levels higher than the dissociation limit at 175 nm for the B state, which is correlated with O(^{1}D) + O(^{3}P). Since O_2 is a major constituent of the atmosphere, the photoabsorption of O_2 in the Schumann−Runge system is important in determining the transmission of the solar radiation in the atmosphere. Photodissociation in the SRC produces O(^{1}D), which is a source for producing free radicals OH and NO in the upper atmosphere. In view of the importance of the photochemistry of the SRC in aeronomy, many experimental[1−6] and theoretical studies[7−11] have been devoted to understanding the dynamics and kinetics of O(^{1}D) produced in the photodissociation of O_2.

The quantum yields of O(^{1}D) were measured by Lee et al. and found to be mostly 1 in the SRC.[1] However, the spectrum was determined by connecting data points measured at many discrete wavelengths. This is adequate in the main continuum between 140 and 170 nm; but it is desirable to scan the spectrum of SRC at the long and short wavelength parts where the variation of quantum yields may happen. For wavelengths below 140 nm, the absorption spectrum consists of discrete structures; a continuous scan in this part of the wavelength is especially necessary.

In the wavelengths below 140 nm, the quantum yields drop below 1 owing to the interaction of the B $^3\Sigma_u^-$ state with other excited states. The electron energy loss experiments by Cartwright et al.,[12] Huebner,[13] Trajmar et al.,[14] and Spence[15] have found evidence for the existence of several states with symmetries of $^3\Pi_u$ or $^3\Pi_g$, which are correlated with two ground state O atoms. Recently the existence of the $^3\Pi_g$ state embedded in the SRC was revealed in an experiment to measure the photoabsorption of O_2 in a cold supersonic beam in the 138−152 nm region.[16] Two-photon laser spectroscopy also revealed the existence of the $^{1,3}\Pi_g$ states.[17−20] To our concern, the one-photon-allowed $^3\Pi_u$ state embedded under the continuum is more important.

The dynamics of the photodissociation of O_2 in producing O(^{3}P$_J$) and O(^{1}D) has been investigated. A branching ratio of the O(^{3}P$_J$) at different J levels was measured at 157 nm.[2−6] O atoms produced in the photodissociation are kinetically hot, and the collisional relaxation of the kinetic energy and angular distribution of O(^{1}D) produced in the photodissociation were investigated recently.[5,6] For example, it was found while Ar was very effective in relaxing the hot atom in both its speed and orientation, the light gas He was useful in relaxing the speed only.

The metastable O(^{1}D) has a long radiative lifetime (120 s).[1] The spectroscopic detection of O(^{1}D) by observing the weak magnetic dipole-allowed radiative transition (^{1}D−^{3}P) at the wavelength 630 nm is difficult. Matsumi et al.[4−6] utilized a LIF technique in the VUV region to excite the metastable atom to an upper electronic state.

Studies of O(^{1}D) may take advantage of the fast reaction as demonstrated by Lee et al.:[1]

$$O(^1D) + O_2 \rightarrow O(^3P) + O_2(b\,^1\Sigma^+_g, v'=0,1) \qquad (1)$$

The production of $v' = 2$ in O_2(b) is endothermic by 23 cm^{-1}.

As was shown previously,[1] the emission of O_2(b−X) at 762 nm with a radiative lifetime of 12 s is easier to detect than the O(^{1}D−^{3}P) at 630 nm.[1,2] This method is also employed in the present experiment to measure the quantum yield of O(^{1}D). Our experiment was designed to scan the entire spectrum at 105−180 nm, but only the results for SRC will be reported in this paper.

2. Experimental Section

The experiment was conducted by using the synchrotron radiation of SRRC at Hsinchu, Taiwan. The synchrotron radiation was dispersed by a 600 GV/mm grating with a 1 m Seya monochromator. There was a LIF window to isolate the experimental cell from the monochromator. Since emission from O_2(b) is relatively weak, resolution was reduced to enhance the fluorescence signal. In this experiment, data were obtained with a resolution of 0.5 nm (300 μm slit with a dispersion 1.65 nm/mm).

* Corresponding author.
† Department of Physics.
‡ Department of Chemistry.
⊗ Abstract published in *Advance ACS Abstracts,* August 1, 1997.

S1089-5639(97)00439-8 CCC: $14.00

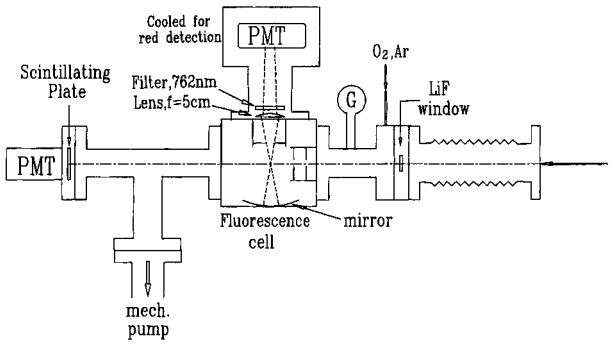

Figure 1. Experimental setup of the detector system.

The 762 nm fluorescence was detected by a cooled photomultiplier tube (PMT) that has a GaAs photocathode (Hamamatsu R666). An interference filter peaked at 761 nm with a fwhm of 10 nm was employed to cut down the background signals. A small lens was employed to focus the fluorescence into the detector. In the fluorescence cell, a concave mirror was placed across the detector to improve the collection of signals by reflecting the outgoing fluorescence back to the detector. Figure 1 shows a sketch of the detector setup.

Cooling the PMT to a temperature of −20 °C effectively reduced the background signal to about 10 count/s with VUV light presented. Depending on the sampling rate, a maximum signal of about 200 counts could be observed at the peak when the synchrotron beam current was just injected (200 mA). However, fluorescence signals less than 50 counts or so were more common when the electron beam current was reduced and scanned at wavelengths other than the maximum peaks. Light source intensity was measured by a second photomultiplier tube with a Na-salicylated coated window in a current mode. All signals were sent to a 486 PC through a GPIB interface.

Experiments were mostly carried out using O_2 pressures of 100−200 mTorr in about 3 Torr of Ar. High-purity O_2 was flushed into a flow cell with an absorption length of about 35 cm. Pressure of the gas was measured by a MKS baratron. Gases were provided by the Cryogenic Gas Company.

3. Results

The absorption cross section was measured by using the Beer's law with an absorption length of 35 cm. The photodissociation cross section σ_d was determined by measuring the fluorescence intensity at 762 nm:

$$S_b = J_0\{\exp(-\sigma_a[O_2]x)\}\sigma_d[O_2]\rho Q \qquad (2)$$

where J_0 is the unattenuated light, σ_a the absorption cross section, x the path length of about 14 cm (the fluorescence cell is located in the middle of the absorption cell), σ_d the photodissociation cross section, ρ the system constant of the system including the efficiency of the PMT, geometric factors such as solid angle, and the transmission of the detector plus filter, and Q the collision-related term. It was important to correct the attenuation of the synchrotron flux, which varied with time and wavelength. In order to get enough fluorescence signal, we kept our experimental pressure above 100 mTorr. The photoabsorption and excitation spectra were obtained by averaging data measured at a oxygen pressure of about 150 mTorr. At this pressure the absorption cross sections agree fairly well with previous data. For wavelengths above 170 nm, the fluorescence signals were weak, and we employed a higher pressure (450 mTorr) to obtain the quantum yield shown in this paper. The spectra of photoabsorption and photodissociation cross sections and their difference are shown in Figure 2.

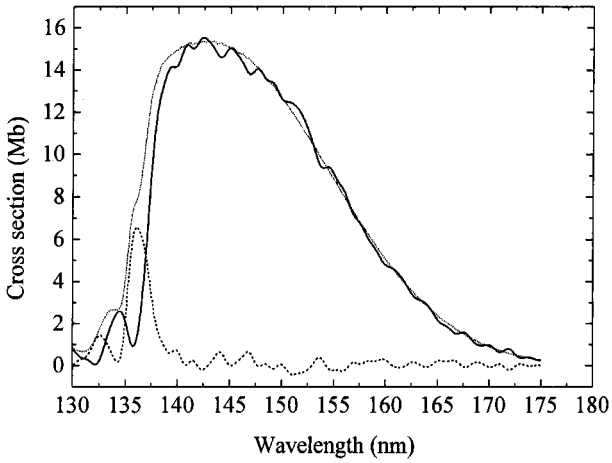

Figure 2. Cross sections of photoabsorption (dotted line), photodissociation of $O(^1D)$ (solid line), and the difference (dashed line) (which corresponds to the state $^3\Pi_u$ in the Schumann−Runge continuum measured in this experiment). 1 Mb = 10^{-18} cm^2.

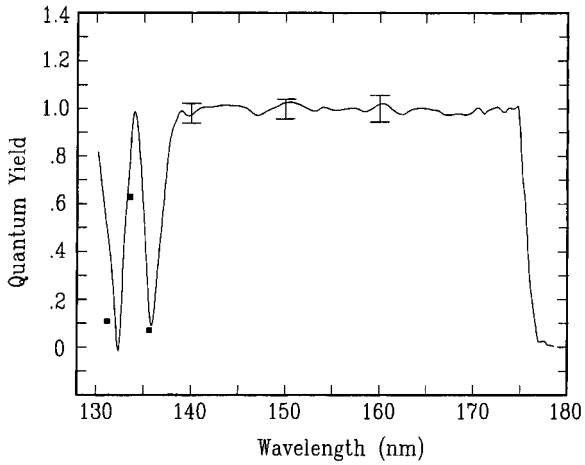

Figure 3. Spectrum of quantum yield of $O(^1D)$ at 130−180 nm of O_2. Squares are data of the maximum and minimum reported in ref 1.

The quantum yield is defined as the ratio between σ_d, the photodissociation cross section, and σ_a, the photoabsorption cross section:

$$Y = \sigma_d/\sigma_a \qquad (3)$$

The quantum yield in SRC was derived in a relative manner. The spectrum of σ_d overlapped the absorption spectrum quite well in the 140−175 nm range, as shown in Figure 2. If we assume a value $Y = 1$ at any point in this spectrum, the absolute quantum yield can be derived. This was actually done by calibrating the data at 155−165 nm assuming unity quantum yield. The averaged values of the system constant in this wavelength range were obtained and used to calculate the quantum yield in the rest of the spectrum, as shown in Figures 2 and 3. The justification of using $Y = 1$ at the wavelengths at about 160 nm is based on both experimental[1,2] and theoretical[10] investigations done before.

We found the 762 nm fluorescence was significantly enhanced by adding Ar to the system. Figure 4 shows the fluorescence excitation spectra measured at various pressures of Ar. The enhancement was also observed for Ne and He. The effect of diffusion of O_2(b) is the cause of this effect, as will be discussed later. The addition of N_2 and Xe significantly reduced the fluorescence signals because of their large quenching rates on $O(^1D)$, as listed in Table 1.

A sample of data at wavelengths for high and low absorption cross sections are given in Table 2 for three oxygen pressures.

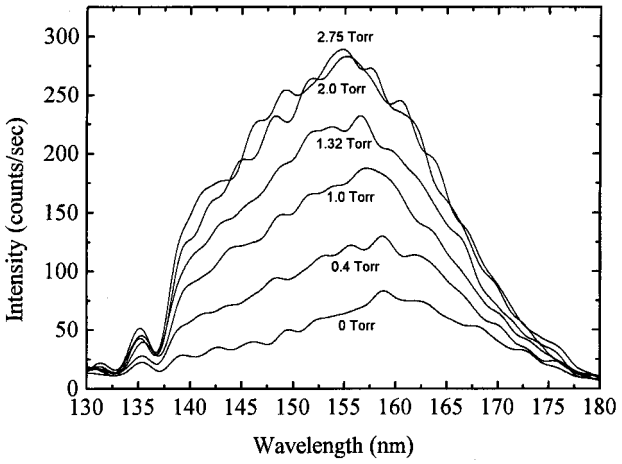

Figure 4. Variation of the 762 nm fluorescence intensity in the Schumann−Runge continuum with different pressures of Ar. Data were measured with 1.7 nm resolution.

In this table, we showed fluorescence signal (count), preabsorption, and quantum yields. Data higher than 300 mTorr were found to be affected by saturation and therefore are not listed.

Errors of the quantum yield measurements mainly resulted from statistical fluctuations in the fluorescence signals. It is estimated the uncertainty was about ±18% in the quantum yield measurements, resulting from the following errors: *S*(fluorescence signal), ±15%; *J*(flux), ±10%; O_2(pressure), ±5%. However, uncertainties at the two particular wavelengths 132.3 and 135.8 nm corresponding to the quantum yield minima, as shown in Figure 3, are expected to be higher. This is due to the low fluorescence signals detected here compared with backgrounds. As shown in Table 2, the background signals at 100 and 164 mTorr are about 16 counts, corresponding to a statistical fluctuation of about 4 counts. However, signals are only 1−2 counts. On the basis of the data at 134.2 nm, which has an unity quantum yield, a yield of 0.1 would generate a signal of 2−4 counts, which is again consistent with measurements.

4. Discussions

A. Kinetics of O(1D) and O_2(b). The O(1D) atom produced in the photodissociation in SRC is kinetically hot. Matsumi et al.[5] investigated the kinetic energy of the hot atoms produced in the photodissociation of O_2 at 157 nm. The noble gases were studied for their relaxation of the translational energy and angular orientation of O(1D). Argon was found to be useful for both purposes.

The translational energy of the hot atom is relaxed in time by constant k_E:[5]

$$\langle E(t)\rangle = \langle E(0)\rangle \exp(-k_E M t) \quad (4)$$

where $\langle E(t)\rangle$ is the average energy at time t, and $k_E = 1.28 \times 10^{-10}$ cm^3/s for Ar and 1.53×10^{-10} cm^3/s for O_2. M is the density of the gas. The time required to thermalize the hot atoms is less than 1 μs. This will take five collisions to bring the hot atoms to thermal velocity based on the following equation:

$$\langle v(n)\rangle = \langle v(0)\rangle \exp(-k_n n) \quad (5)$$

where $\langle v(n)\rangle$ is the velocity after n collisions, and $k_n = 0.39$/collision for Ar.[5]

The advantage of using Ar as the buffer gas is for its smaller electronic quenching rate but large translational energy quenching rate.[5,6] The gas O_2 also slows down diffusion; however, O_2 significantly quenches O(1D). At low pressure, O_2 is helpful in improving the fluorescence signal by vibrational quenching of the O_2(b,v'=1) to O_2(b,v'=0) according to the previous studies.[21] The rate constants of the relevant processes are listed in Table 1. We also calculated the loss rate (time constant) for each reaction.

The existence time for O(1D) in the system is very short since it is converted into O_2(b) in about 1 μs, as shown in Table 1. Since there is more Ar(3 Torr) in the system than O_2(0.15 Torr), O(1D) is relaxed before it reacts with O_2. After being formed, O_2(b) can survive for a long time since it is not easily quenched by any gas as shown in Table 1. The radial diffusion of O_2(b) becomes important. It can be shown that Q in eq 2 is proportional to radial diffusion time τ_r, which can be calculated with the diffusion constant D:

$$D = \lambda\langle v_b\rangle/3 \quad (6)$$

where λ is the mean free path and $\langle v_b\rangle$ is the mean speed for O_2(b). Calculations give $D = 0.06$ m^2/s for 0.15 Torr of O_2 and 0.003 m^2/s for 3 Torr of Ar. The detector had a viewing zone with dimensions about 1 cm (beam direction) × 0.5 cm (width) × 1 cm (field depth). The radial diffusion distance r_D for a time Δt is estimated as follows:[26]

$$r_D = (2D\Delta t)^{1/2} \quad (7)$$

Δt is estimated to be 1 ms by using a flow velocity of 1000 cm/s. The radial distance r_D is therefore about 1 cm at 0.15 Torr and 0.05 cm at 3 Torr. The radial diffusion is thus appreciable at low pressure (0.15 Torr of O_2) and is negligible at high pressure (3 Torr of Ar). The radial diffusion time constant can be calculated using eq 7 by setting $r_D = 0.5$ cm. It should also be independent of wavelength.

The rate constant k_1 for the energy transfer between O(1D) and O_2 may also depend on the kinetic energy. Although there is so far no such study reported in the literature, we can understand the problem from the temperature dependence of the electronic quenching rate for O(1D) by O_2.[6,23,24] The quenching rate was found to have a negative temperature dependence, and the formation of a complex (O_3) during the collision was proposed. Thus a smaller rate k_1 at higher kinetic energy may happen, and the process can be wavelength dependent in our experiment. However, this effect can be removed by addition of Ar to kinetically relax the hot atoms.

B. Quantum Yields. From Figure 3, we found the quantum yield drops from unity starting from the wavelengths longer than about 175 nm. The dissociation threshold is located at 57136.4 ± 0.9 cm^{-1}, as reported by Gibson et al., who carried out the measurement at a higher resolution by using a VUV laser.[2] The threshold wavelength determined experimentally at room temperature is not expected to be sharp due to excitation of the ground state molecules with high rotational quantum numbers at room temperature. The photoabsorption of the molecules in high rotational states produces O(1D) and would occur beyond the photodissociation threshold. Photoabsorption cross sections of the high rotational molecules were calculated by Lewis et al.[28] A detailed spectrum showing the dissociation and quantum yield near the threshold at 175 nm is given in Figure 5. The threshold wavelengths for different rotational states are also labeled. The decrease of quantum yield in the wavelengths longer than 175 nm corresponds to a decrease of the populations of the rotationally excited molecules that can be excited. The quantum yield was measured to be zero at about

TABLE 1: Rate Constants for Reactions Relevant to This Paper

	gas	type[a]	notation	rate constant (cm^3/s)	ref	loss rate, τ^b (s)
$O(^1D)$	Ar	e quenching	k_2	3×10^{-13}	20	1×10^{-4}
	Ar	t quenching	k_a	1.28×10^{-10}	5	2.5×10^{-7}
	O_2	e quenching	k_3	8.0×10^{-12}	20, 23, 24	2.6×10^{-5}
	O_2	e energy transf.	k_1	3.2×10^{-11}	20, 21	6.5×10^{-6}
	O_2	t quenching	k_4	1.53×10^{-10}	5	1.3×10^{-6}
	N_2	e quenching	k_5	2.6×10^{-11}	20, 24	1.3×10^{-6}
	Xe	e quenching	k_6	7.2×10^{-11}	20	4.3×10^{-7}
$O_2(b)$						
$v' = 1$ to $v' = 0$	O_2	v quenching	k_7	2.2×10^{-11}	21	9.5×10^{-6}
$v' = 0$	O_2	e quenching	k_8	3.9×10^{-17}	22	5.3
$v' = 0$	N_2	e quenching	k_9	2.0×10^{-15}	25	1.5×10^{-2}
	Ar	e quenching	k_{10}	1.5×10^{-17}	22	2.2

[a] e, electronic; v, vibrational; t, translational. Calculation based on $[O_2] = 150$ mTorr, the other gases 1 Torr,[b] $1/\tau = (1/[O(^1D)])\, d[O(^1D)]/dt = k[M]$.

TABLE 2: Data Samples for O_2 at 100, 164, and 233 mTorr[a]

			(1) 100 mTorr			
λ (nm)	132.3	134.2	135.8	140.0	150	155−165
sig. (counts/s)[b]	14	25	16	38	39	22−52
transmission	0.94	0.89	0.71	0.52	0.57	0.67−0.90
quantum yield	0.01	1.23	0.16	0.93	0.98	1(0.14)
			(2) 164 mTorr			
λ (nm)	132.3	134.2	135.8	140.0	150	155−165
sig. (counts/s)[c]	13	27	17	43	61	30−71
transmission	0.90	0.83	0.58	0.34	0.40	0.52−0.84
quantum yield	−0.02	0.93	0.11	1.03	1.01	1(0.08)
			(3) 233 mTorr			
λ (nm)	132.3	134.2	135.8	140.0	150	155−165
sig. (counts/s)[d]	14	39	16	45	58	33−73
transmission	0.86	0.76	0.45	0.21	0.27	0.40−0.78
quantum yield	0.00	1.01	0.04	0.97	0.99	1(0.08)
average quantum yield of (1)−(3)	−0.01	1.06	0.10	0.97	0.98	1

[a] Signals were the average of three data files measured at each pressure. In the table, transmission is determined by using a path length of 14 cm. In the last column, the range of wavelength (155−165) is given where data were averaged to get unity quantum yield (with fluctuation given in the parentheses) used for calibration as described in the text. The signal and transmission are given by the maximum and minimum values measured in this wavelength range. [b] Background 14 counts. [c] Background 15 counts. [d] Background 16 counts.

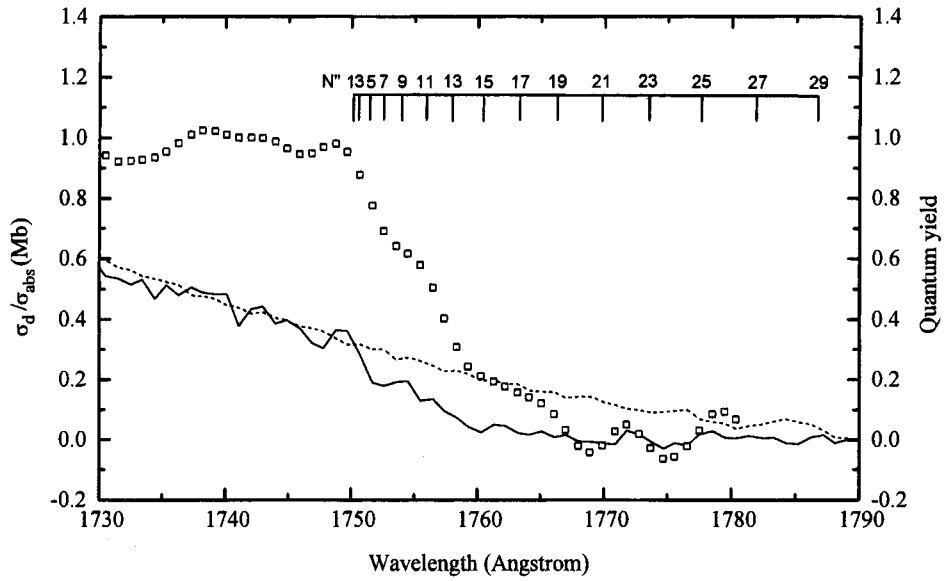

Figure 5. Photoabsorption (dashed line), photodissociation (solid line), and quantum yield (squares) spectra near the photodissociation threshold for $O(^1D)$ production at 175 nm. Threshold energies corresponding to different rotational states of the molecules in the ground electronic state are labeled according to Lewis et al.[28]

177 nm; the difference from the thermal threshold at 175 nm is 2 nm, which is greater than the spectral resolution (0.5 nm).

Quantum yield falls off rapidly below about 140 nm. Previously, several studies have attempted to deconvolute the SRC absorption.[11,27] Variation of the quantum yield is caused by the production of two ground state O atoms. Sominska et al.[16] assigned bands observed in the 138−155 nm region to the $^3\Pi_g$ state by using a supersonic oxygen beam. According to these authors, the forbidden transition to the g state was made possible under the influence of clusters, which should not be a concern in our studies. Instead, the state $^3\Pi_u$ which produces two ground state O atoms should be responsible for the

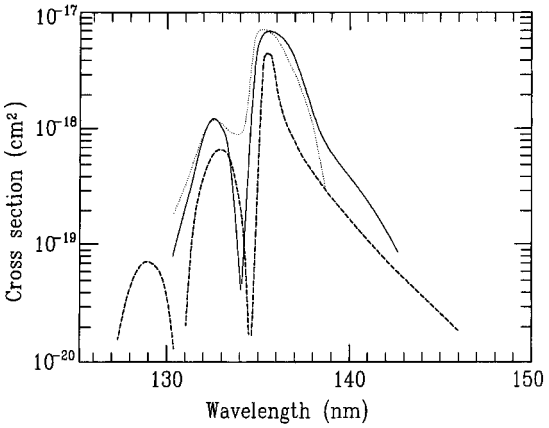

Figure 6. Absorption spectrum of $^3\Pi_u$ from three different authors. Solid line: our data, determined by subtraction of photodissociation cross section σ_d from the absorption cross section σ_a shown in Figure 1. Dashed line: theoretical calculations of Allison et al.[10] Dotted line: data from ref 1.

underlying state near 136 nm.[10] A subtraction of the photodissociative cross section from the absorption cross section was tried to derive a spectrum for $^3\Pi_u$, as shown in Figure 2. An enlarged spectrum for $^3\Pi_u$ compared with other studies is shown in Figure 6. Note that the cross section maxima in Figure 6 corresponds to the minima in Figure 2 or Figure 3 since they ($^3\Sigma_u$ and $^3\Pi_u$) are just opposite in producing O(1D).

Our quantum yield below 140 nm roughly agrees with the previous measurement.[1] The first major difference is at the peak 134.2 nm with the quantum yield of 1 for O(1D) (or zero for $^3\Pi_u$), compared with the peak at 133.6 nm with a yield of about 0.6 in the previous experiment.[1] This band should be a pure $^3\Sigma_u$. The 135.8 minimum ($Y = 0.1$) is the same for both experiments within the uncertainty of the resolution. But we have a minimum quantum yield at 132.3 nm ($Y = 0$) corresponding to a complete $^3\Pi_u$ absorption. However, nonzero values were reported in the previous experiment. We thus confirmed completely the previous measurement in the main continuum, but only partially in the structured spectrum.

Our band positions and cross sections for the $^3\Pi_u$ state are very similar to the theoretical calculation of Allison et al.[10] The significance may be the wavelength positions of unity and null quantum yield for O(1D), which corresponds to a complete signature of the $^3\Sigma_u$ or $^3\Pi_u$ state, respectively. Both states interact strongly with each other. The peak positions for the $^3\Pi_u$ state are given in Table 3.

5. Conclusions

Quantum yields of O(1D) from photodissociation of O_2 were measured in the Schumann−Runge continuum at 130−175 nm. The quantum yield was found to be 1 at 140−175 nm, but varies from 1 at both the long and short wavelength ends of SRC. Near the threshold, 175 nm, the quantum yield decreases slowly, which is caused by the excitation of the rotationally excited O_2. For wavelengths shorter than about 139 nm, the quantum yield was found to vary from maximum (1) to minimum (0) at a few wavelength positions resulting from the crossing of the $^3\Pi_u$ state with the B $^3\Sigma_u^-$ state.

TABLE 3: Cross Sections of Maximum and Minimum Absorption for the State $^3\Pi_u$ (The Maximum Here Corresponds to the Minimum in $^3\Sigma_u$); Quantum Yields Are Shown in Table 2

references	max. wavelength (nm)	min. wavelength (nm)
This work	135.8, 132.3	134.2
Allison et al.[10]	135.5, 132.9	134.5
Lee et al.[1]	135.6, 131.2	133.6

The 762 nm fluorescence from the transition O_2(b−X) produced by the energy transfer from O(1D) was enhanced with increasing of the Ar pressure. The effect is caused by the reduction of the diffusion of the O_2(b) produced from O(1D). Kinetics of the relevant processes are discussed.

Acknowledgment. This research is supported by Grant NO. NSC85-2112-M008-012. We acknowledge technical support by the staff of SRRC.

References and Notes

(1) Lee, L. C.; Slanger, T. G.; Black, G.; Sharpless, R. L. *J. Chem. Phys.* **1977**, *67*, 5602.
(2) Gibson, S. T.; Lewis, B. R.; Baldwin, K. G. H.; Carver, J. H. *J. Chem. Phys.* **1991**, *94*, 1060.
(3) Huang, Y.; Gordon, R. J. *J. Chem. Phys.* **1991**, *94*, 2640.
(4) Matsumi, Y.; Kawasaki, M. *J. Chem. Phys.* **1990**, *93*, 2481.
(5) Matsumi, Y.; Shamsuddin, S. M.; Sata, Y.; Kawasaki, M. *J. Chem. Phys.* **1994**, *101*, 9610.
(6) Matsumi, Y.; Chawdhury, A. M. S. *J. Chem. Phys.* **1996**, *104*, 7036.
(7) Saxon, R. P.; Liu, B. *J. Chem. Phys.* **1997**, *67*, 5432.
(8) Buenker, R. J.; Peyrimhoff, S. D. *Chem. Phys. Lett.* **1975**, *34*, 225.
(9) Friedman, R.; Du, M. L.; Dalgarno, A. *J. Chem. Phys.* **1990**, *93*, 2370.
(10) Allison, A. C.; Guberman, S. L.; Dalgarno, A. *J. Geophys. Res.* **1992**, *87*, 923.
(11) Li, Y.; Honigmann, M.; Bhanuprakash, K.; Hirsch, G.; Buenker, R. J.; Dillon, M. A.; Kimura, M. *J. Chem. Phys.* **1992**, *96*, 8314.
(12) Cartwright, D. C.; Hunt, W. J.; Williams, W.; Trajmar, S.; Goddard, W. A., III. *Phys. Rev. A* **1973**, *8*, 2436.
(13) Huebner, R. H.; Celott, D. C.; Mielczarek, S. R.; Kuyatt, C. E. *J. Chem. Phys.* **1975**, *63*, 241.
(14) Trajmar, S.; Cartwright, D. C.; Hall, R. I. *J. Chem. Phys.* **1976**, *65*, 5275.
(15) Spence, D. *J. Chem. Phys.* **1981**, *74*, 3898.
(16) Sominska, E.; Kelner, V.; Gedanken, A. *Chem. Phys. Lett.* **1993**, *213*, 117.
(17) van der Zande, W. J.; Koot, W.; Los, J. *J. Chem. Phys.* **1989**, *91*, 4597.
(18) Peterson, J. R.; Bae, Y. K. *Phys. Rev. A* **1984**, *30*, 2807.
(19) van der Zande, W. J.; Koot, W.; Peterson, J. R.; Los, J. *J. Chem. Phys.* **1988**, *126*, 169.
(20) Schofield, K. *J. Photochem.* **1978**, *9*, 55.
(21) Lee, L. C.; Slanger, T. G. *J. Chem. Phys.* **1978**, *69*, 4053.
(22) Lawton, S. A.; Phelps, A. V. *J. Chem. Phys.* **1978**, *69*, 1055.
(23) Amimoto, S. T.; Force, A. P.; Gulotty, R. G., Jr.; Wissenfeld, J. R. *J. Chem. Phys.* **1979**, *71*, 3640.
(24) Streit, G. E.; Howard, C. J.; Scheltekipf, A. L.; Davidson, J. A.; Schiff, H. I. *J. Chem. Phys.* **1976**, *65*, 4761.
(25) Kohse-Hoinghaus, K.; Stuhl, F. *J. Chem. Phys.* **1980**, *72*, 3720.
(26) Atkins, P. W. *Physical Chemistry*, 4th ed.; Oxford University Press: Oxford, England, 1990.
(27) Cartwright, D. C.; Fiamengo, N. A.; Williams, W.; Trajmar, S. *J. Phys. B* **1976**, *9*, L419.
(28) Lewis, B. R.; Berzins, L.; Carver, J. H.; Gibson, S. T. *J. Quant. Spectrosc. Radiat. Transfer* **1985**, *33*, 627.